







A Late Devonian coelacanth reconfigures actinistian phylogeny, disparity, and evolutionary dynamics

Received: 5 December 2023

Accepted: 2 August 2024

Published online: 12 September 2024

 Check for updates

Alice M. Clement ^{1,10} ✉, Richard Cloutier ^{1,2,3,10}, Michael S. Y. Lee^{1,4}, Benedict King⁵, Olivia Vanhaesebroucke², Corey J. A. Bradshaw ⁶, Hugo Dutel ⁷, Kate Trinajstić ^{8,9} & John A. Long ^{1,9,10}

The living coelacanth *Latimeria* (Sarcopterygii: Actinistia) is an iconic, so-called ‘living fossil’ within one of the most apparently morphologically conservative vertebrate groups. We describe a new, 3-D preserved coelacanth from the Late Devonian Gogo Formation in Western Australia. We assemble a comprehensive analysis of the group to assess the phylogeny, evolutionary rates, and morphological disparity of all coelacanths. We reveal a major shift in morphological disparity between Devonian and post-Devonian coelacanths. The newly described fossil fish fills a critical transitional stage in coelacanth disparity and evolution. Since the mid-Cretaceous, discrete character changes (representing major morphological innovations) have essentially ceased, while meristic and continuous characters have continued to evolve within coelacanths. Considering a range of putative environmental drivers, tectonic activity best explains variation in the rates of coelacanth evolution.

Coelacanths are evolutionarily unique, lobe-finned fishes that first appeared in the fossil record in the Lower Devonian Period (late Lochkovian, ~419–411 million years ago [Ma])¹, with over 175 fossil taxa described throughout the Palaeozoic and Mesozoic eras. Since the discovery of *Latimeria chalumnae* by Western scientists in 1938, the phylogenetic relationships among coelacanths have been investigated in more than 20 studies (see Supplementary Text for full list). In most analyses, a good congruence exists between the phylogeny and the stratigraphic record. Coelacanths are considered to be morphologically conservative in terms of body plan^{2–7} and they achieved a peak of diversity during the Triassic^{6,8–11}. Meanwhile, rates of morphological evolution have been examined stratophenetically¹² and phylogenetically^{3,9,13}, indicating that there was an early burst of

evolution during the Devonian followed by a precipitous decrease and then a steady, low rate of morphological evolution. However, no driver has ever been proposed to explain these distinctive evolutionary dynamics of coelacanths, nor has their status as ‘living fossils’ been quantitatively evaluated.

Devonian coelacanth material is rare, representing only a small component of the ~175 fossil coelacanth species—there are only 20 known taxa, about half of which are too incomplete to describe formally. Their earliest fossils (Early Devonian) are known from mostly isolated bones from the late Lochkovian and Pragian of China^{1,14} and the mid–late Pragian of Australia¹⁵. Most Devonian coelacanths are rare and fragmentary, except for the middle Frasnian *Miguashaia bureaui* from eastern Canada^{16,17}, and the late Famennian *Serenichthys kowiensis*¹⁸

¹College of Science and Engineering, Flinders University, Adelaide 5042, Australia. ²Département de Biologie, Chimie et Géographie, Université du Québec à Rimouski, Rimouski G5L 3A1, Canada. ³Excellence Center in Evolution of Life, Basin Studies and Applied Paleontology, Palaeontological Research and Education Centre, Mahasarakham University, Maha Sarakham 44150, Thailand. ⁴Earth Sciences Section, South Australian Museum, North Terrace, Adelaide 5000, Australia. ⁵Max Planck Institute for Evolutionary Anthropology, Deutscher Platz 6, 04103 Leipzig, Germany. ⁶Global Ecology | Partuyarta Ngadluku Wardli Kuu, College of Science and Engineering, Flinders University, Adelaide 5001, Australia. ⁷University of Bristol, School of Earth Sciences, Bristol, UK. ⁸School of Molecular and Life Sciences, Faculty of Science and Engineering, Curtin University, Perth 6845, Australia. ⁹Earth and Planetary Sciences, Western Australian Museum, 49 Kew Street, Welshpool 6106, Australia. ¹⁰These authors contributed equally: Alice M. Clement, Richard Cloutier, John A. Long.

✉ e-mail: alice.clement@flinders.edu.au

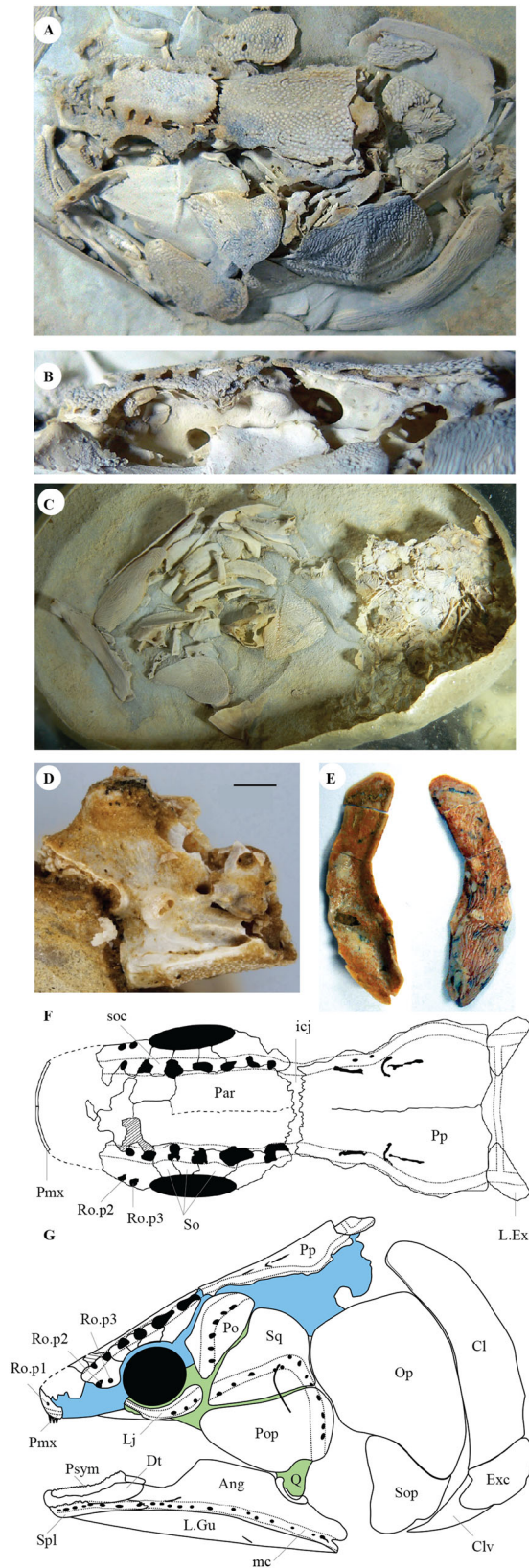


Fig. 1 | Acid prepared material and skull reconstruction of *Ngamugawi wirngarri* gen. et sp. nov. **A, B** 'Part a' of WAM 09.6.148 (holotype) shown in left dorsolateral view and skull close up in left lateral view. **C** 'Part b' of WAM 09.6.148 (holotype) showing all exposed elements; **D** partial braincase of NMV P231504 (paratype) shown in right lateral view; **E** cleithrum of NMV P231504 (paratype) in mesial and lateral view; **F, G** skull reconstruction in dorsal and left lateral view. Abbreviations: Ang angular, Cl cleithrum, Clv clavicle, Dt dentary, Exc extra-cleithrum, icj intracranial joint, ioc infraorbital canal, L.Gu lateral gular, Lj lachrymojugal, mc mandibular canal, L.Ex lateral extrascapular, Op operculum, Par Parietal, Po postorbital, Pop preoperculum, Pp postparietal, Pmx premaxilla, Psym parasymphysial, Q quadrate, Ro.p1 anterior pore of the rostral organ, Ro.p2 antero-lateral pore of the rostral organ, Ro.p3 postero-lateral pore of the rostral organ, So supraorbitals, soc supraorbital canal, Sop Suboperculum, Spl splenial, Sq squamosal.

Formation of Australia^{20–25}. Exceptional 3-D preservation of our specimens facilitates rare insight into the neurocranial, branchial, and palaeoneurological conditions of the group. These data also allow us to re-evaluate the phylogeny and phenotypic evolution of all coelacanths in detail, using an expanded character matrix, as well as the first geometric morphometric study of the group to our knowledge, and an analysis of putative drivers of evolutionary rates. Along with this description, such an expansive time series of detailed evolutionary patterns for a single taxon extending right up to the present offers an opportunity to determine the global processes steering evolution more generally.

Results

Systematic palaeontology

Osteichthyes Huxley 1880

Sarcopterygii Romer 1955

Actinistia Cope 1871

Ngamugawi wirngarri gen. et sp. nov.

Etymology. Generic name meaning “ancient fish” in Gooniyandi/Guniyandi, language of the First Nations people from Country around Fitzroy Crossing in the Kimberley region of Western Australia. Specific name is given in honour of respected Gooniyandi elder and ancestor Wirngarri, who lived in the Emanuel Range. Generic and specific names were both provided to Prof. John Long in September 2023, who has a longstanding and ongoing relationship with the community, with permissions to use the language granted by elder Rosemary Nuggett, on behalf of the Gooniyandi people of the Mimbi community.

Holotype. The holotype (WAM 09.6.148; Figs. 1, 2) is a small but mostly complete skull (measuring just over 2 cm in length) with all dermal skull bones, an intact neurocranium, gill-arch skeleton, and pectoral girdle preserved in close articulation. The anterior section of the body is also present comprising many scales and vertebral arch elements, but the pectoral fin and its endoskeleton are missing.

Referred material. The paratype (NMV P231504; Figs. 1, 2) contains associated elements comprising two cleithra, the ventral portion of the basisphenoid and parasphenoid, and several isolated scales.

Locality and horizon. Canning Basin, in northern Western Australia, circa 100 km southeast of Fitzroy Crossing; Gogo Formation, early Frasnian, Late Devonian (–384–382 Ma). The holotype was found between Stromatoporoid Camp and Longs Well, the paratype was found in Paddys Valley (see map of Gogo fossil localities in figure 1 within ref. 23).

Diagnosis. *Ngamugawi wirngarri* gen. et sp. nov. is distinguished from all other coelacanths by the following apomorphies: jugal canal with prominent branches; large sensory pore openings between supraorbitals and parietals; teeth on parasymphysial tooth plate, but not on

based on juvenile specimens from South Africa. Until now, *Diplocercides kayseri*¹⁹ from Gerolstein in Germany is the only Devonian coelacanth known from three dimensions (3-D) and revealing part of the neurocranium, but it has since been destroyed by serial grinding.

The material presented here, comprising two specimens (Fig. 1), represents the first-known coelacanth from the Late Devonian Gogo

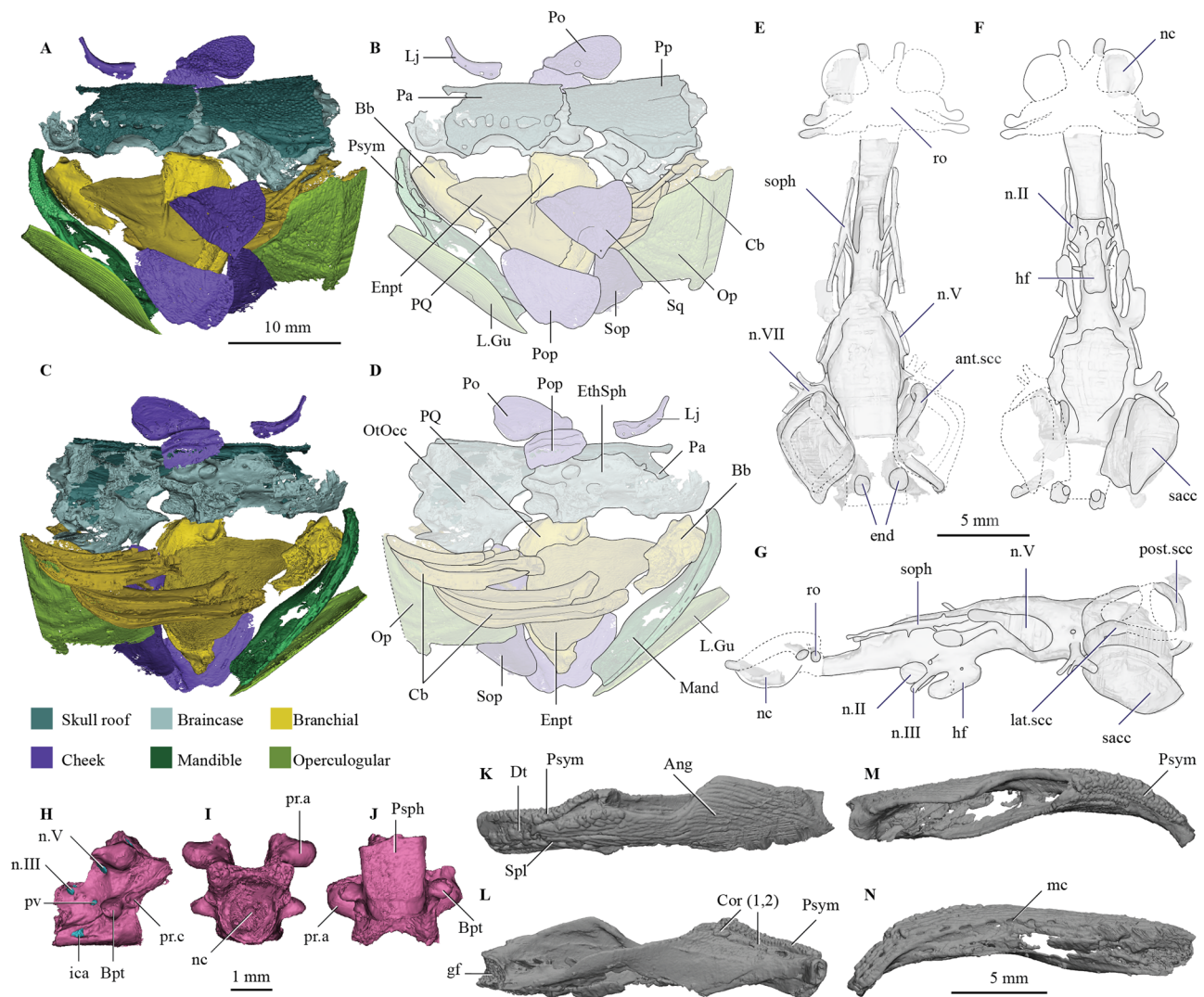


Fig. 2 | Volume renderings of high-resolution μ CT scans showing 3D anatomy of select elements of *Ngamugawi wirngari* gen. et sp. nov. A–D ‘Part a’ of WAM 09.6.148 (holotype) shown in two views; **E–G** cranial endocast reconstruction from WAM 09.6.148 in dorsal, ventral and left lateral view; **H–J** partial braincase of NMV P231504 (paratype) shown in left lateral, posterior and ventral views; **K–N** left mandible of WAM 09.6.148 (holotype) shown in left lateral, medial/mesial, dorsal and ventral views. Abbreviations: Ang Angular, ant.scc anterior semicircular canal, Bb basibranchial, Bpt Basipterygoid process, Cb ceratobranchial Cor coronoids, Dt dentary, end canals for endolymphatic ducts, Enpt entopterygoid EthSph

ethmosphenoid, hf hypophysis, ica canal for internal carotid artery, lat.scc lateral semicircular canal, L.Gu lateral gular, Lj lachrymojugal, n.I–VII cranial nerves I to VII, Mand mandible, nc nasal capsule, nc notochordal canal, Op operculum, OtOcc otico-occipital, Pa parietal, Po postorbital, Pop preoperculum, Pp postparietal, post.scc posterior semicircular canal, PQ palatoquadrate, pr.a antotic process, pr.c processes connectens, Psph parasphenoid, Psym parasymphysial, pv canal for pituitary vein, ro rostral organ, sacc sacculus, Spl Splenial, Sq squamosal, soph canal for superficial ophthalmic nerve. All CT data and models are available via: www.morphosource.org/projects/000485769?locale=en.

the dentary; prearticular and/or coronoid teeth rounded; cleithra and extracleithra with broad triangular anteroventral overlap for clavicle bearing a large ventral foramen; and scales with long ornamental ridges extending beyond the posterior margin of the base (Figs. 1, 2, Supplementary Fig. 1).

This published work and the nomenclatural acts it contains have been registered in ZooBank, the proposed online registration system for the International Code of Zoological Nomenclature (ICZN). The ZooBank LSIDs (Life Science Identifiers) can be resolved and the associated information viewed through any standard web browser by appending the LSID to the prefix “<http://zoobank.org/>”. The LSIDs for this publication are: B2B4AA94-E9A5-4D05-9724-CBE5B54760EA; 567A96D6-654A-4201-BFDB-0D81BBBF6226.

Description

The holotype (WAM 09.6.148) was fossilised in an inter-reef palaeoenvironment with the dorsal surface of the skull roof in contact with the

substrate, so that during decay the lower jaws and some cheek elements disarticulated, resting anterior to the skull, while the snout has collapsed inwards. The main block (part A) contains the complete skull including neurocranium, left mandible, cheek, pectoral girdle, and branchial elements, while the counterpart (block B) includes the parasphenoid and right-side mandibular ramus, operculum, entopterygoid, as well as a complete set of branchial arches. The specimen lacks the posterior portion of the body.

The well-preserved skull roof is ornamented with enamel-capped tubercles. The well-developed dorsal lamina of the premaxilla is pierced by a single large opening for the anterior tube of the rostral organ, which is diagnostic for coelacanth. There are paired parietals and postparietals partially fused in their anterior half, preparietals, and no pineal opening (Figs. 1, 2). The parietals and postparietals are approximately equidimensional in length each about 10 mm long (parietal length \div postparietal length = 0.8252; mean = 0.7824, $n = 47$ coelacanth species). The parietal/postparietal ratio varies greatly

among Devonian coelacanths: ranging from 0.38 for *Diplocercides kayseri*²⁶, 0.51 for *Serenichthys kouiensis*¹⁸, to 0.70 for *Miguashaia bureaui*¹⁷. The preorbital, orbital, and postorbital regions of the ethmoidal shield (parietonasal shield) make up 48%, 34%, and 18% of the total length of the shield, respectively, consistent with the proportions of “anatomically modern coelacanths” *sensu* Zhu et al.¹⁴ with elongate preorbital and orbital regions. There are six or seven supraorbitals preserved as in *D. kayseri*²⁶; the posteriormost supraorbital corresponds most likely to a fusion of two or three elements. The supraorbital sensory canal passes through the sutures between the supraorbitals and the parietals, with 7–8 large pores opening through the skull roof highlighting its lyre-shaped course (Fig. 1). Narrow tabulars are fused to the postparietals.

Similar to other Devonian coelacanths (e.g., *Gavinia*, *Miguashaia*, *Diplocercides*), the cheek region of *Ngamugawi* is long compared to post-Devonian coelacanths. The postorbital, squamosal, preopercular, and lachrymojugal bones are arranged as in *D. kayseri*^{26,27} and *Serenichthys*¹⁸ in having the squamosal and preoperculum set atop one another, the postorbital farther anteriorly, and an elbow-shaped lachrymojugal expanded ventrally and bearing large, medial sensory pores as in *D. kayseri*. The sub-oval postorbital has a short orbital margin and bears six infraorbital sensory canal pores. Unlike the condition in *Serenichthys*, *Gavinia*, and post-Devonian coelacanths, whereby the postorbital anterior margin is long and curved to fit behind the orbit, in *Ngamugawi* the orbital margin is short as in *D. heiligenstockensis*²⁷ and *M. bureaui*¹⁷. The squamosal is sub-triangular and bears a vertical cheek pit line posteroventrally, and pores for the jugal and preopercular sensory canals. The preoperculum is trapezoidal, with four or five large pores of the preopercular canal, and abuts the squamosal ventrally, yet is separated from the lachrymojugal. The operculum bears a distinctive, strong ridge running anteroposteriorly through the bone, with a series of associated foramina likely to be the “epibranchial line” of Northcutt²⁸ as in *M. bureaui*¹⁷.

The lower jaw of *Ngamugawi* is distinctive, with a long dentary (40% of the mandible length), a long splenial, a unique arrangement of coronoids, and lacking a dentary sensory pore (Fig. 2K–N). The dentary is unusually long compared to most other coelacanths (35% of the mandible length), but similar to the proportion of the dentary observed in the most primitive coelacanth *Styloichthys* (50%) as well as some Carboniferous taxa (e.g., *Rhabdoderma elegans* 40%; *Cardosuctor populosum* 43%; *Allenpterus montanus* 42%). Unique among coelacanths, *Ngamugawi* has a large, denticulated (not ‘toothed’, nor bearing ‘pointed teeth’) bone sutured medially to the dentary, which we interpret as a parasymphysial bone (Fig. 1G). Enlarged parasymphysials are also found in onychodontids and porolepiforms, so we propose that the specific position and elongation of this bone is a sarcopterygian synapomorphy. There are three equidimensional coronoids, and an additional, enlarged principal coronoid. The angular bears an oral pit-line in its anterior half and some large sensory pores along its ventral margin. The prearticular bone lacks elongate ridges in its ventral portion. The glenoid fossa has a single posterodorsally facing facet, and the Meckelian bone bears an articulation point for the symplectic posteriorly. The left lateral gular is long and flat, only slightly shorter than the mandible as in most coelacanths. It has a small pit-line located posterior to the centre of the bone as in *D. heiligenstockensis*²⁹ and *Chagrinia enodis*³⁰.

The braincase of *Ngamugawi* is exceptionally well-preserved in 3-D (Figs. 1B, D, 2A–D, H–J), and is the best-preserved braincase known for a Palaeozoic coelacanth. Much of the braincase is well-ossified, preserving most of the ethmosphenoid and otico-occipital, with the unossified areas of the braincase where cartilage prevailed precisely matching the same regions of cartilage formation in *Latimeria*³¹. The braincase, cranial endocast, and palate bears many similarities to that of *D. kayseri*²². The interorbital cartilage is ossified. The processus connectens extends to the level of the antotic process and does not

meet the parasphenoid. The antotic processes are large and teardrop-shaped, whereas the basiptyergoid processes are smaller and knob-like. The occipital area appears to have been less-ossified than more anterior portions and might have been cartilaginous as in *Latimeria*³³. The posterolateral wall of the otico-occipital bears a distinct, short otic process not seen in any other coelacanth, nor sarcopterygian. Two endolymphatic ducts face dorsally, opening through the endoskeletal cranial roof (Fig. 2E). The parasphenoid forms an elongate ‘spatulate’ outline as in *Diplocercides*^{17,34}, with a gently rounded anterior margin and covered in a denticle field that ends abruptly posterior to the internal carotid foramen (Supplementary Fig. 2E–H). The parasphenoid is medially concave with an open buccohypophyseal canal. The entopterygoids are sub-triangular with a broad posterior flange as in other coelacanths. They are smooth laterally but ridged across most of their palatal surface.

The nasal capsules are shallow and rounded, situated in line with the cranial cavity as in many sarcopterygians (contra *Latimeria*). The general proportions of the rostral organ can be reconstructed from the position of the pore openings and by comparison with that of *Latimeria*³³ (Fig. 2E–G). The olfactory tracts seemingly travelled through the large common anterior section of the endocranial cavity, rather than via separate olfactory tracts as in dipnomorphs and tetrapodomorphs. Canals for the optic nerves (n.II), oculomotor nerves (n.III), and trochlear nerves (n.IV) all exit the cranial cavity laterally. Those of the trochlear nerves travel just over a millimetre anterolaterally before meeting the superficial ophthalmic canals. The hypophysial fossa is short compared to that of juvenile and adult *Latimeria* specimens³³. It extends anteroventrally as in that taxon but lacks an obvious posterior lobe as in *Diplocercides kayseri*³². There is no evidence of pineal or parapineal recesses. The endocast is narrow in the ethmosphenoid region but broadens from the level of the intracranial joint to reach its maximum width anterior to the labyrinths (Fig. 2E–G). Posterior to this, a large canal for the facial nerve (n.VII) exits the braincase laterally before splitting into three branches, and a canal for the auditory nerve (n.VIII) leads into the labyrinths.

The inner-ear region and the posterior portion of the endocast are more poorly ossified and were likely cartilaginous as in *Latimeria*³³. Two long, open endolymphatic ducts are situated at the posterior of the skull roof. Anterior and posterior semicircular canals are preserved on the right-hand side of the specimen, and portions of the external semicircular canal and the sacculus are preserved on the left (Fig. 2E–G). The labyrinth region shows a large ampulla on the anterior semicircular canal, but the condition for the other two is unknown. The sacculus appears to have been large and deep as in *Diplocercides*, with the sinus superior not projecting above the cranial cavity dorsally.

Ngamugawi contains the best-preserved visceral skeleton of any Palaeozoic coelacanth (Supplementary Fig. 1G, H). While most of the visceral skeleton is preserved as a thin, ossified perichondral layer, we note an ossified hyomandibular is absent; we consider this due to it being cartilaginous as in *Latimeria*. The anterior end of the urohyal forms a single point, but the posterior bifurcation of the urohyal is pronounced as in most coelacanths. The single basibranchial has parallel lateral margins, and the ceratohyal is long and narrow. Five ceratobranchials are strongly curved and expanded proximally, while the epibranchials are triradiate, rod-like elements similar to those of *Latimeria chalumnae*.

Within the pectoral girdle, the cleithrum, extracleithrum, and clavicle form a prominent postbranchial lamina (Fig. 1E, G; Supplementary Fig. 1I). The cleithra are rounded dorsally, bear a ridged ornament, have a distinct anterior groove for the articulation of the operculum, and are partially fused with the broad extracleithrum (a synapomorphy of coelacanths). There is a broad, triangular anteroventral overlap between the extracleithrum and the clavicle. A large foramen lies on the visceral surface on the smooth overlap area for the clavicle lateral surface. The triangular clavicle is short as in *Miguashaia*.

The sigmoid anocleithrum bears no ornament and has an anteriorly-pointed tip with an articular facet.

The scales are either teardrop-shaped, similar to *Lualabaea* or *Caridosuctor*³⁵, or ovate, with a longitudinal, ridged enamel ornament. The spiny apices of the thicker ridges protrude from the posterior margin of the scales (Supplementary Fig. 1D); this feature seems to be unique to *Ngamugawi* among coelacanths. Lateral line scales have large pore openings. There are no bumps on the inner surface of the scales as for *Miguashaia*^{17,35}.

Although the two specimens are small, they likely represent adults based on the presence of many fusions between bones, the degree of ossification of the branchial elements, and the degree of development of the scales.

Phylogenetic and Evolutionary Analyses

First, we evaluated the phylogenetic position of *Ngamugawi wirngari* gen. et sp. nov. via Bayesian inference and maximum parsimony using an exhaustive and greatly expanded data matrix of 87 species (82 coelacanths and 5 onychodontiform outgroups) coded for 322 total characters (268 discrete, 14 meristic, and 40 continuous – see Supplementary Text for detailed description of all characters and analyses and Supplementary Fig. 3 for the position of the 88 landmarks for the 40 continuous characters). These matrices combine characters from 16 previous analyses including Forey's⁹ classic matrix (some original characters have been deleted, split, or redefined; Forey's matrix has been used in 20 analyses so far), in addition to 85 new characters. Autapomorphies (unique characters of terminal taxa) have been scored and coded. We double-checked all characters for each taxon, validating or invalidating previous coding. Both Bayesian inference (Fig. 3) and maximum parsimony (Supplementary Fig. 6) recover broadly congruent topologies: *Ngamugawi* is recovered as sister taxon to *Gavinia*, crownward of *Miguashaia* spp. and *Holoptyerygius*, and basal to *Diplocercides* and *Serenichthys*. *Styloichthys* is sister taxon to all other coelacanths.

Bayesian tip-dating revealed a striking uncoupling between rates of evolution of discrete, meristic, and continuous character types. The uncorrelated log-normal clock (which allowed all branches to have separate rates: Fig. 4) and the epoch clock (which constrained rates to be the same within time slices: Supplementary Fig. 6) retrieved similar patterns. We found that coelacanths experienced a rapid burst of morphological evolution with the highest rates occurring early in their history during the Devonian Period, but these rates then slowed substantially (with rare exceptions). Discrete characters, which often reflect evolutionary innovations, virtually stopped evolving after the Cretaceous (Fig. 4D); the substitution tree reveals *Latimeria* has undergone no more anagenesis than Cretaceous relatives, i.e. for discrete characters, it has indeed been frozen in evolutionary time. In contrast, meristic and continuous characters, which often reflect changes in proportions, have continued to evolve at typical Mesozoic rates (Fig. 4E-F). There are other instances of uncoupled rates of evolution for different character types: *Holoptyerygius* and *Allenkypterus* exhibit fast rates for continuous and meristic changes, but unremarkable rates for discrete characters. These are explicable, e.g., *Holoptyerygius* and *Allenkypterus* are unusually shaped coelacanths, but have retained most typical coelacanth traits.

Next, we constructed a resampled boosted regression tree analysis to identify the relative contribution of five putative palaeoenvironmental drivers to rates of coelacanth evolution: namely, subduction flux; continental flooded area (incorporating percentage of shallow sea); sea surface temperature; atmospheric CO₂; and dissolved O₂ (see Supplementary Information 3a) (Fig. 5). We used a combined rate of evolution, considering the discrete, meristic, and continuous characters, for each species (i.e., the rate associated exclusively to the species on the leading phylogenetic branch). The resampled final trees had high coefficients of variation (a measure of goodness of fit)

ranging from 48% to 91%. Of the putative environmental drivers considered, the influence of subduction flux (a proxy of tectonic activity) was the most strongly associated environmental measure to the rate of evolution (median relative influence = 36%; range = 13–60%) – thus, indicating that coelacanth species evolved more rapidly during periods of higher global tectonic activity (Fig. 5B), suggesting that the creation of new habitats favoured rapid morphological evolution. The percentage of continental flooded area (Fig. 5C) had the next-highest explanatory power, albeit considerably lower than subduction flux (median relative influence = 24%; range = 2–46%). There was little support for a relationship between the remaining environmental drivers (atmospheric CO₂, sea surface temperature, dissolved O₂) and the rate of coelacanth evolution (Fig. 5).

Lastly, we evaluated disparity of coelacanth morphology using two approaches: (i) principal coordinates analysis (PCoA) applied to the discrete phylogenetic matrix (with missing data for each coelacanth species reconstructed using parsimony), and (ii) principal component analysis (PCA) of the 2-D geometric morphometrics to analyse shape of the body, lower jaw, and cheek (Fig. 6; Supplementary Fig. 7). Variation in body shape and lower jaw are conservative^{2,3,9}, while the cheek region is more variable among species (or disparate)^{3,9,36}.

For the principal coordinates analysis of discrete characters, we recovered a profound shift in overall disparity between Devonian and all post-Devonian coelacanths, but the highest disparity (discrete) during the Devonian and Triassic (Fig. 6A; Supplementary Fig. 8A). Again, *Latimeria* appears to have moved little outside the morphospace of its closest Mesozoic relatives, despite having an additional 66 million years to evolve, consistent with the stasis for discrete characters found in the tip-dated phylogenetic analyses.

For the principal component analysis of overall body shape (Fig. 6B; Supplementary Fig. 8B), the Devonian *Miguashaia bureaui*, the Carboniferous *Allenkypterus montanus*, and the Triassic *Foreyia maxkuhni* are three outliers highly modified in body shape compared to the generalised coelacanth body type, accounting for approximately 35% of the total variation. A second source of body-shape variation considers the discrepancies associated with the heterocercal and triphycercal caudal fins (Supplementary Fig. 9A). A major shift of disparity occurred between Devonian and post-Devonian species. *Latimeria* is positioned away from its closest Mesozoic relatives, again consistent with the lack of stasis found for continuous (shape) characters in the tip-dated phylogenetic analyses. The disparity in the cheek region offers a distinct pattern of temporal evolutionary disparity. Two temporal shifts characterized the cheek disparity (Fig. 6C; Supplementary Fig. 8C): one post-Devonian (narrowing of the cheek, Supplementary Fig. 9B) and the second between the Triassic and Jurassic (deepening of the cheek, Supplementary Fig. 9B). The disparity of the cheek region is greater than that of body shape and lower jaw, while the disparity of the lower jaw is slightly greater than that of the body shape and shows a relatively constant temporal overlap (Fig. 6D, Supplementary Fig. 10).

Discussion

Ngamugawi shows characteristics intermediate between 'anatomically primitive' (e.g., *Styloichthys*, *Miguashaia*) and 'anatomically modern' (e.g., *Diplocercides*, *Euporoosteus*, and post-Devonian species) coelacanths *sensu* Zhu et al.¹⁴, both in its phylogenetic position and morphological disparity. Phylogenetically, *Ngamugawi* is closely related to another Australian Devonian coelacanth – *Gavinia* – both are basal to *Diplocercides* and *Serenichthys*, and post-Devonian coelacanths. Anatomically modern coelacanths were thought to be characterized by two pairs of parietals (i.e., one pair of parietals and one pair of pre-parietals), enlarged preorbital and orbital regions of the ethmosphenoid shield (~40% preorbital, 50% orbital, and 10% postorbital regions), and a trilobate tail (i.e., triphycercal caudal fin)¹⁴, features absent in 'anatomically primitive' forms. *Ngamugawi* bears one pair of

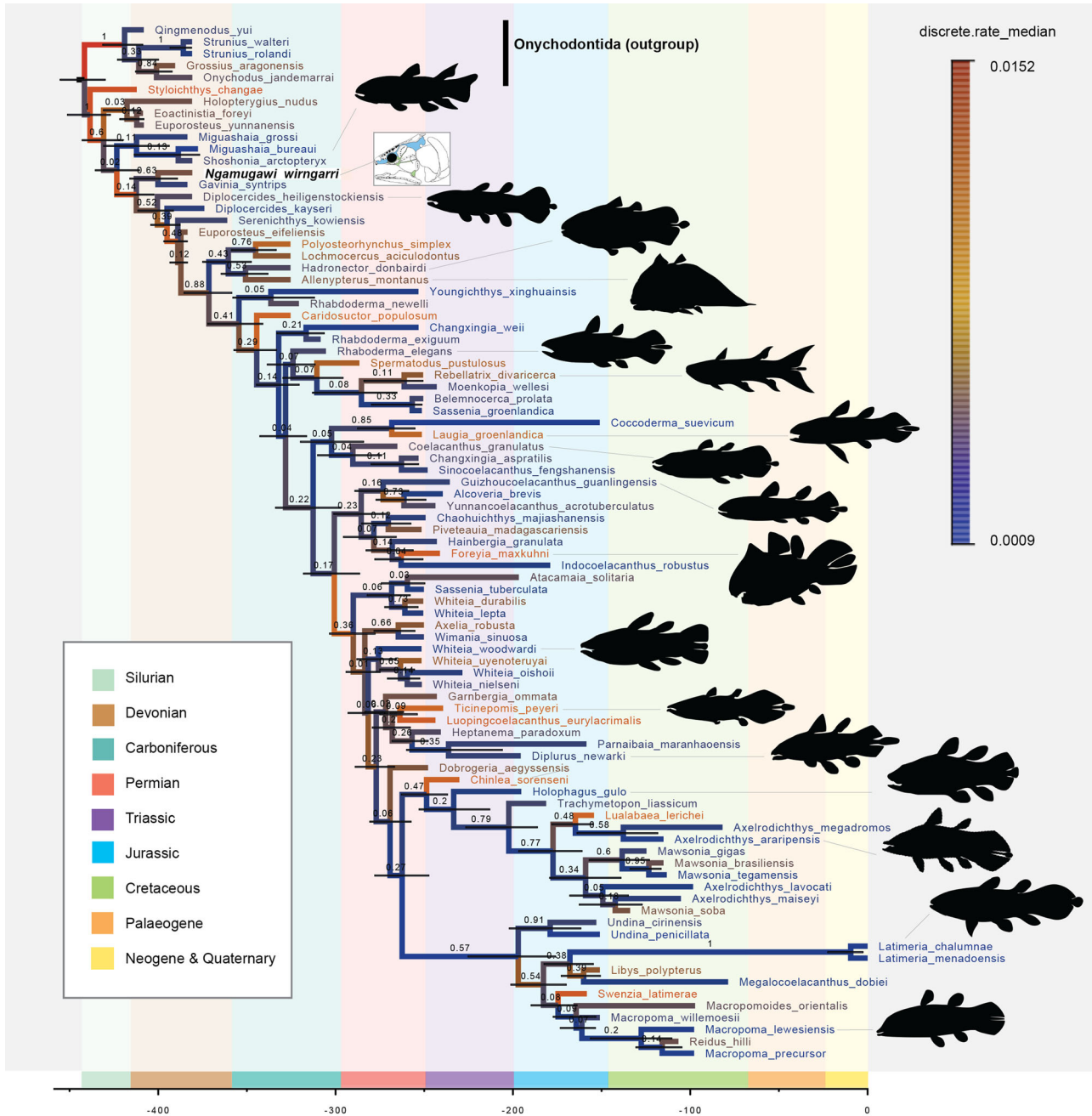


Fig. 3 | Phylogenetic relationships and divergence dates within coelacanth, based on tip-dated Bayesian inference. *Ngamugawi wirngarri* gen. et sp. nov., shown in enlarged black text. Each branch is coloured according to median rate of morphological evolution of discrete characters under the uncorrelated lognormal

relaxed clock (details in Fig. 4). Numbers at branches refer to posterior probability. Identification of, and credit for, the coelacanth silhouettes is provided in Supplementary Fig. 4.

parietals and preparietals, but the proportions of the three ethmosphenoid regions are intermediate between the so-called ‘primitive’ and ‘modern’ coelacanth (48%, 34%, and 18%). Furthermore, *Miguashaia bureaui* was considered anatomically primitive¹⁴, due to features inferred in its reconstruction¹⁷, such as the presence of a heterocercal caudal fin and the proportions of the ethmosphenoid shield (34%, 21%, and 45%). However, new *M. bureaui* material shows an ethmosphenoid condition more intermediate between ‘anatomically primitive’ and ‘modern’ coelacanth (51%, 30%, and 19%). Thus, the gap between ‘anatomically primitive’ and ‘anatomically modern’ coelacanth is now bridged, leaving only *Styloichthys* discriminated from all remaining coelacanth. *Ngamugawi* was crucial to this interpretation, and thus holds a key position in the early evolution of coelacanth (with most

other taxa in this region of the tree being poorly known). The undistorted, 3-D-preserved neurocranium of *Ngamugawi wirngarri* thus provides valuable insight into the neurobiological evolution of early coelacanth more generally.

The detailed analyses of evolutionary rates also substantiate the ‘living fossil’ status of *Latimeria*, but with important nuances. After the Mesozoic, there was a sharp decline in rates of evolution of discrete characters, but rates in meristic and continuous (i.e., shape) traits have not declined; these patterns are also reflected in the morphospace analyses of discrete characters and body shape. Discrete characters often refer to evolutionary innovations, such as the presence or absence of novel structures that are difficult to encapsulate as meristic or continuous traits. In contrast, meristic

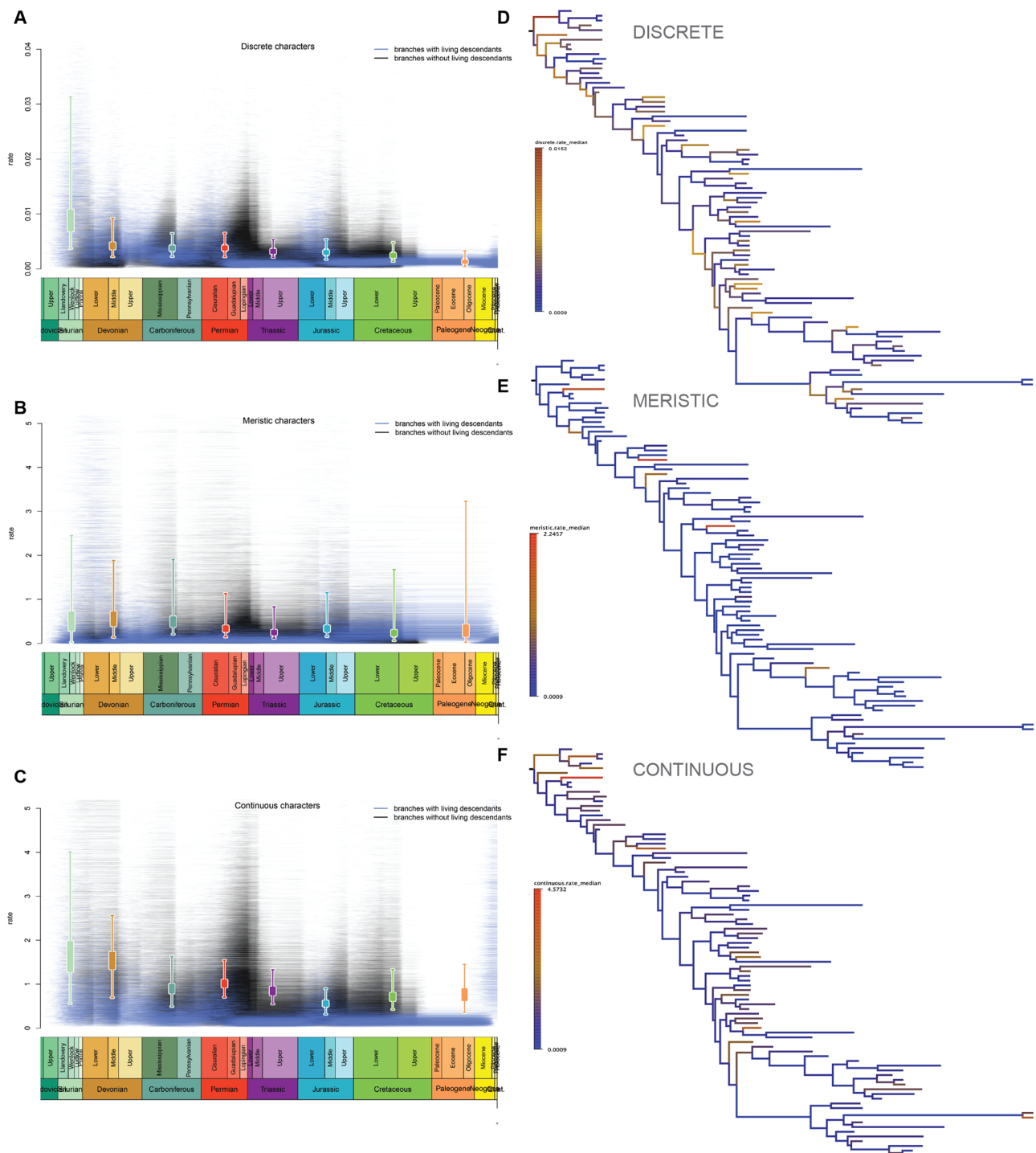


Fig. 4 | Results based on Bayesian total-evidence tip dating under the uncorrelated lognormal clock; there is a sharp slowdown in discrete character evolution in the most recent time bin, but no such slowdown for meristic or continuous characters. Rates of evolution through time for **A** discrete, **B** meristic, and **C** continuous characters; each plot shows the duration and rate for every branch in the MCMC tree sample. Median rates for each branch for **D** discrete, **E** meristic, and **F** continuous characters; taxon labels for trees are as in Fig. 3. Due to

constraints in BEAST2, absolute rates of change are shown for discrete characters, but relative rates (weighted average = 1) shown for meristic and continuous characters. In **A–C**, fuzzy plots depict branch rates in 1000 MCMC tree samples (8000 post-burnin trees, thinned by factor of 8); box and whisker plots depict inter-quartile (50%) and range for the average rate in each sample for the relevant geological period. In **D–F**, branch rates are median rates for 8000 post-burnin trees.

and continuous characters typically refer to more subtle evolutionary changes in proportions. Thus, a biological interpretation of the rate results is that, since the Cretaceous, coelacanths have largely ceased evolving major innovations (discrete characters), yet finer-scale tinkering (meristic and continuous characters) has continued unabated, as indeed has genomic evolution^{37,38}. Hence,

coelacanths might indeed be considered living fossils due to their lack of major recent innovations, but in more subtle features and their DNA³⁸, they have continued to evolve at more normal rates for vertebrates. Although slowly evolving organisms, higher rates of global tectonic activity appear to have been one of the main putative abiotic drivers of faster rates of morphological

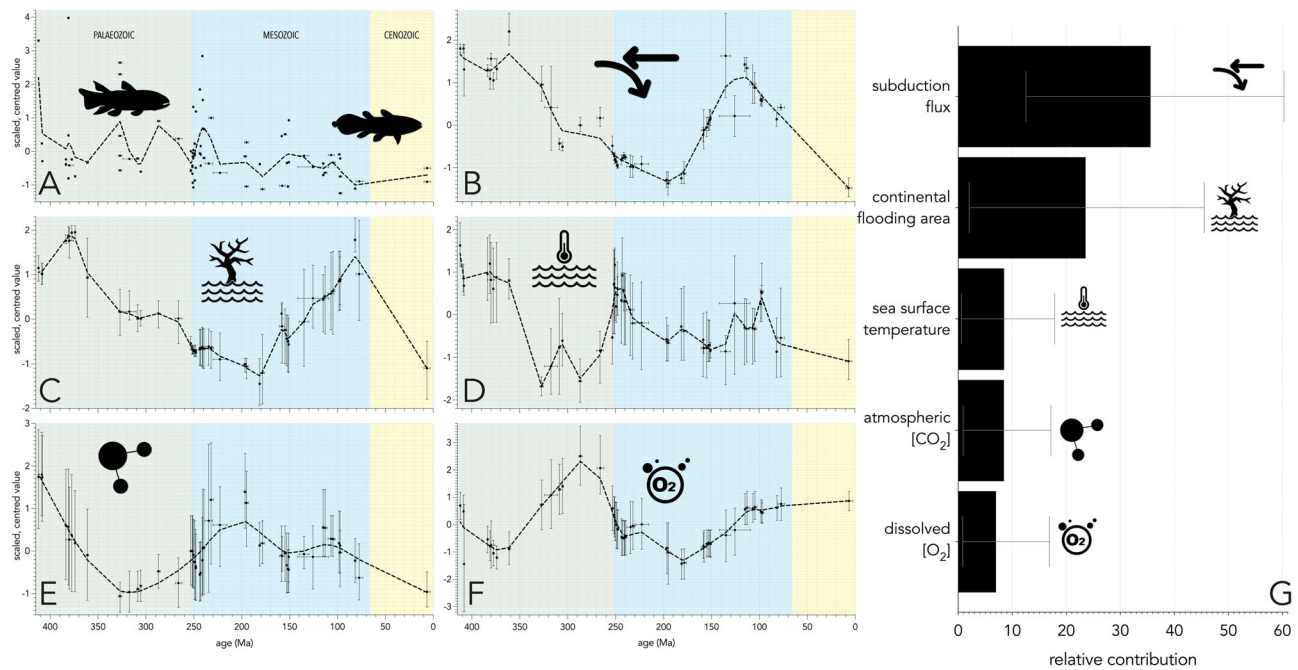


Fig. 5 | Temporal trends in environmental drivers of coelacanth evolutionary rates, showing that, of the variables measured, subduction flux had the greatest influence on coelacanth evolution overall. A Scaled and centred rate of evolution of all coelacanths, **B** subduction flux; **C** continental flooded area (incorporating % shallow seas), **D** sea surface temperature; **E** atmospheric CO₂ concentration, **F** dissolved (marine) O₂, and **G** relative influence of each environmental

driver on rate of coelacanth evolution. x-axis error bars in A-F are standard errors derived from the source literature, y-axis error bars are 95% confidence limits; error bars in G represent 95% confidence limits and are derived from 1000 iterations of the boosted regression tree analysis. Green = Palaeozoic, blue = Mesozoic, yellow = Cenozoic.

evolution in coelacanths by facilitating episodes of biogeographic differentiation.

Methods

Material

Both specimens were collected during the 2008 Museum Victoria Gogo Expedition led by JAL and funded by the Australian Research Council. Landowners and leaseholders gave permission to do field work, and no additional permits were required under the Lands Administration Act. The specimens are registered in the collections of the Western Australian Museum as WAM 09.6.148 (holotype) and Museum Victoria as NMV P231504 (paratype). David Pickering and John A. Long (MV) extracted the specimens from their limestone matrix using repeated 10% acetic acid baths, with newly exposed bones strengthened with Paraloid/Mowital B30 in ethanol. JAL dusted specimens with a sublimate of ammonium chloride prior to photography and drew illustrations using a camera lucida.

Computed tomography

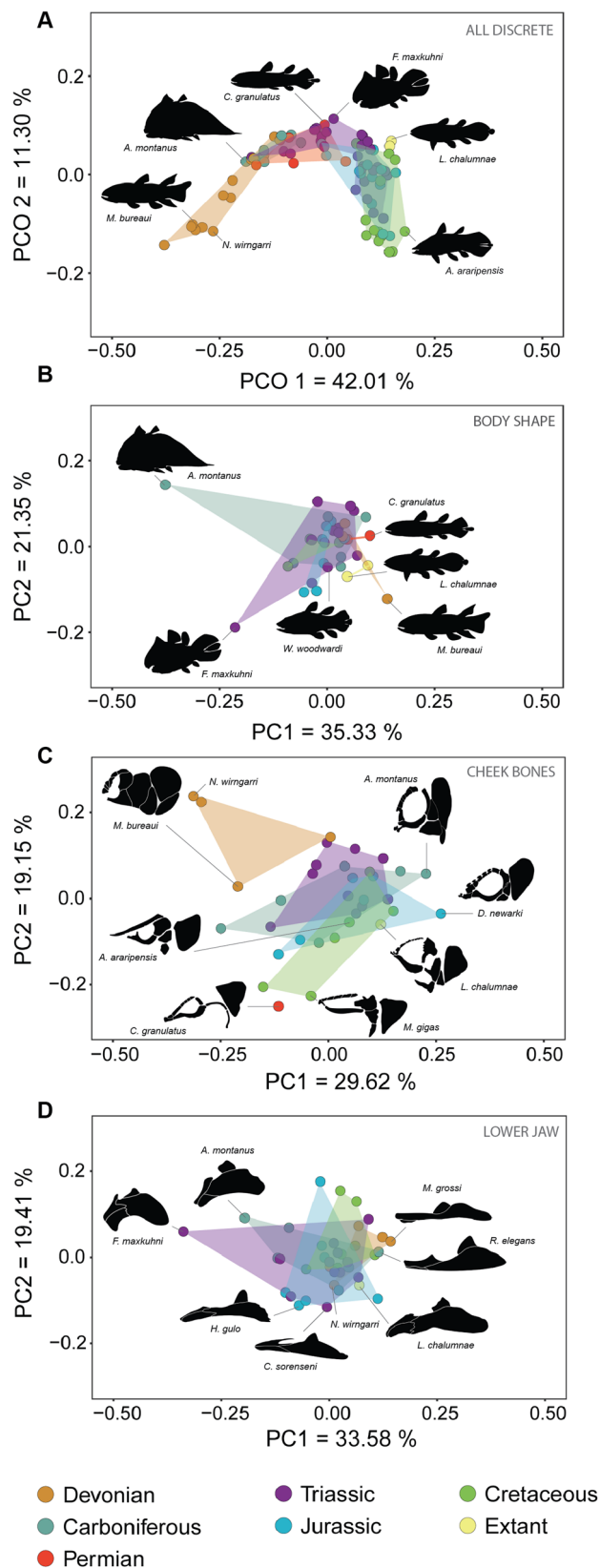
We were granted permission to CT scan the material by Rosemary Nuggett, on behalf of the Gooniyandi people of the Mimbi community, and Mikael Siversson of the Western Australian Museum. We imaged part and counterpart (parts A & B) of the holotype WAM 09.6.148 at the Australian National University (ANU) X-ray Micro-CT Laboratory. Later, we (re)imaged the holotype (part A) and the paratype MV P231504 at the Adelaide Microscopy CT Facility (University of Adelaide) on a Skyscan1076 X-ray microtomography scanner using the following parameters: holotype, 74 kV; 135 μA; 0.5 mm aluminium (Al) filter; 360° rotation at 0.4° increments; frame averaging = 2; 2.4 second acquisition time; and paratype, 100 kV; 70 μA; 1.0 mm aluminium (Al) filter; 360° rotation at 0.4° increments; 3 frames/rotation; 4.1 second acquisition time. The resultant pixel size for the initial holotype scan was 150 μm, the paratype was 9 μm, and the holotype (part a) rescan was 17 μm. We reconstructed the resultant 16-bit depth TIFF images

using the Skyscan NRecon software (Bruker microCT, Belgium), after which we completed 3-D segmentation and rendering using Mimics v.19.0 (biomedical.materialise.com/mimics; Materialise, Leuven, Belgium). Skull reconstruction was done in 3-matic (Materialise, Leuven, Belgium), and animations assembled using Adobe Premier Pro. Scan data and all resulting 3-D models (STLs) and animations are available via MorphoSource (www.morphosource.org/projects/000485769?locale=en), as well as the Github repository github.com/cjabradshaw/CoelacanthEvolution/.

Phylogenetic analyses

To assess the phylogeny, we compiled three phylogenetic matrices for 82 coelacanth species and five onychodontiform outgroups containing 268 discrete, 14 meristic, and 40 continuous characters (see Supplementary Information for detailed description of all characters). Detailed description of the characters, states, scores and sources is provided in the supplementary information. We applied Bayesian (BEAST2) and maximum parsimony analyses (TNT) to create a newly proposed phylogeny. The discrete matrix is available on MorphoBank (Project 3471), the meristic and continuous characters are available at <https://doi.org/10.5281/zenodo.8054092>.

Bayesian tip-dated analyses. We were performed Bayesian tip-dated analyses using BEAST 1.10.5³⁹ (BEAST2 currently cannot accommodate continuous traits with missing data). The data were explicitly gathered to satisfy the assumptions of tip dating, namely sampling all variable traits, including autapomorphies (see Supplementary Information). The most appropriate available tree prior was the birth-death serial-sampling model (BDSS⁴⁰); the alternative SABD tree prior is only available in BEAST2⁴¹. The optimal evolutionary histories that explain the discrete, meristic and continuous traits, as well as stratigraphic dates, were inferred using Markov-chain Monte Carlo (MCMC) approaches, as implemented in BEAST. The executable XML files, with annotations describing model, prior, MCMC run and



logging settings, and R scripts, are available in Github <https://github.com/cjabradshaw/CoelacanthEvolution>. Four runs of all analyses were conducted, with run lengths and burnin confirmed as adequate for convergence using Tracer⁴²; the post-burnin samples of all 4 runs were then combined and summarised using post-processing BEAST modules LogCombiner and TreeAnnotator⁴³ as well as R scripts

Fig. 6 | Discrete and morphometric disparity of coelacanths. **A** Principal coordinates analysis plot showing principal coordinate 1 versus principal coordinate 2, disparity based on discrete characters for all coelacanth taxa ($n = 82$ species). **B–D** Principal component analysis plot showing principal component 1 versus principal component 2 disparity based on 2-D geometric morphometrics for **B** body shape ($n = 35$ species); **C** cheek bones ($n = 34$ species); and **D** lower jaw shape ($n = 38$ species). Time-binned morphospaces per geological period compare the distinctiveness, similarity, and temporal evolution of the morphological disparity of coelacanths over a period of 410 Ma. Larger morphospaces indicate greater morphological disparity; overlapping morphospaces indicate similar body plans. There are distinct morphospaces for Devonian and post-Devonian coelacanths. *Latimeria* falls close to its closest, Mesozoic relatives for discrete characters (**A**) and cheek shape (**C**) but is quite distantly separated from Mesozoic forms for overall body shape (**B**) and lower jaw shape (**D**). All individual species data points plotted and identified in Supplementary Fig. 8. Identification of coelacanth silhouettes is provided in Supplementary Fig. 4 (complete body) and Fig. 11 (cheek region and lower jaw).

available in scripts/evolrate using libraries disparity⁴⁴, phytools⁴⁵, phylotate⁴⁶ and geoscale⁴⁷.

Tip calibrations were employed using the full stratigraphic range (including uncertainty) for each species; taxa from the same deposit were constrained to co-vary in age by putting a tight (exponential) prior on their age variance (cf^{48}). The maximum root age was unconstrained, but there was an exponential prior putting 95% of probability distribution between the oldest sampled fossil (412.15 Ma) and the oldest unequivocal sarcopterygians (418 Ma). Trees were rooted with five onychodontiform outgroup taxa.

Discrete morphological characters were analyzed using the Mk_v-model which corrects for non-sampling of constant characters⁴⁹. Multistate characters that formed clear morphoclines (characters 1, 2, 6, 8, 10, 15–16, 23, 26, 36, 53, 60, 74, 76, 97, 100, 110, 112, 135, 137, 208, 218, 224, 227, 240, and 258) were treated as ordered; others were treated as unordered. Among-character rate variation was modelled using the gamma parameter⁵⁰. A state-partitioned model was employed, with substitution rates scaled by state number to correct for state (= base) frequencies (see King et al.⁵¹).

Meristic characters were analyzed using a high-state ordered Mk-model. Essentially, meristic characters were treated as ordered multi-state characters with very large numbers of states, the possible states being the minimum observed value, the maximum observed value, and all intervening whole numbers. Changes between any two states were constrained to pass through all intervening values (states). The large number of states for some characters required the use of unorthodox state labels, which are detailed in the Supplementary Information.

Continuous characters were log-transformed (to base 10) to reduce heteroscedasticity where relevant (highly right-skewed). The transformed data were then analysed using Brownian motion models implemented in BEAST³², with the average evolutionary rate (i.e., variance) for each continuous character estimated separately.

Rate variation across the tree was modelled using two different clock models; in the main analyses, rate variation was estimated separately for the discrete, meristic and continuous characters to test for concordance in patterns.

Uncorrelated lognormal (UCLN) relaxed clock. This clock model assumes rates vary independently across branches, with the values approximating a lognormal distribution with variance estimated from the data⁵³. To achieve convergence, these analyses had to be performed using MC3 methods (4 chains, delta 0.08). The dated tree from this clock model is shown in Fig. 3, along with the estimated rates of discrete, meristic and continuous characters across time (in Fig. 4 and Supplementary Fig. 5).

For testing correlates of evolutionary rates, where it was desirable to have a single rate value for all 3 types of traits, the UCLN relaxed

clock analysis was repeated with discrete, meristic and continuous data modelled under a single (i.e., linked) clock.

Epoch clock. This clock model assumes rates vary independently across time slices, but rates in all branches within each time slice are the same⁵⁴. Branches spanning multiple time slices are allocated multiple rates (i.e., the segment of branch within time slice *a* is allocated the rate for time slice *a*, etc.). Seven epochs were employed: Devonian (and earlier), Carboniferous, Permian, Triassic, Jurassic, Cretaceous, and Tertiary. The rates of evolution for discrete, meristic, and continuous characters across the seven epochs is shown in Supplementary Fig. 5.

Parsimony analyses. Parsimony analyses used TNT⁵⁵ included the discrete, meristic and continuous characters (scaled to the same weight as binary characters), with outgroup and ordering assumptions as above. In order to remove negative log values (unreadable by TNT), all continuous characters had +2 added; the magnitude of the addition makes no difference under parsimony. Searches involved 1000 TBR replicates holding 100000 trees at each step. The strict consensus tree was calculated for all taxa, and with the three most unstable taxa pruned⁵⁶ (Supplementary Fig. 6). Clade support was calculated using 200 bootstrap replicates. The executable TNT files are in Github at <https://doi.org/10.5281/zenodo.8054092>.

Boosted regression trees

We also built boosted-regression trees to test the relationship between rate of coelacanth evolution and five putative environmental drivers, namely subduction flux⁵⁷, continental flooded area (combined with percentage of shallow seas)^{58,59}, sea surface temperature⁵⁷, dissolved O₂⁶⁰ atmospheric CO₂⁶¹ (see Supplementary Information for data collection for these parameters) to account for potential nonlinearity in the relationships. We hypothesised that the rate of evolution would increase within relatively higher concentrations of dissolved O₂ given its suggested role in the evolution of animal life during the Phanerozoic⁶² (but see Schachat^{63,64}). We further hypothesised that variation in atmospheric CO₂ might have influence coelacanth evolution given its role in modifying climate⁶⁵ and the flow of trophic energy through ecological networks⁶⁶. We predicted that relatively higher sea surface temperatures would indicate higher rates of coelacanth evolution given the positive influence of temperature on poikilotherm metabolism⁶⁷. Finally, we predicted that increasing subduction flux⁵⁷, a measure of relative tectonic activity, would facilitate episodes of biogeographic differentiation and influence patterns of speciation^{65,68} through the exploitation of novel niches, and that a higher percentage of shallow seas globally would provide more opportunity for evolution since most coelacanth species have been discovered mainly in marine and estuarine palaeoenvironments^{9,69,70}.

We also accounted for potential phylogenetic non-independence and temporal autocorrelation by resampling the dataset 1000 times using the following procedure: (i) we constructed a temporal vector of ages by Gaussian-resampling the mean and standard deviation of the intervals between fossil appearance periods (based on the first and last appearances) using one-third of the calculated standard deviation and removing the negative intervals; (ii) for each resampled temporal sequence, we determined which species appeared within the sequence points (again, based on first and last appearances), (iii) for each of the species within the resampled sequence, we resampled a random uniform value for each putative environmental driver between its maximum and minimum, and (iv) we transformed, centred, and scaled the extracted environmental values using the *scale* function in R. For each of these 1000 resampled datasets, we ran a boosted regression tree emulator to predict the rate of coelacanth evolution (scaled, centred, log₁₀-transformed itself to produce a Gaussian-like distribution) from the scaled environmental variables using a learning rate = 0.0003,

tolerance = 0.00005, error family = Gaussian, bag fraction = 0.75, tree complexity = 2, and maximum number of trees = 1,000,000 in the function *gbm.step* from the *dismo* R library⁷¹. For each of the 1000 iterations, we retained the coefficient of variation as a measure of goodness of fit, the relative influence of each environmental variable, and the predicted relationship between scaled rate of evolution and each scaled environmental variable, from which we estimated 95% confidence limits using the *quantile* function in R. However, we also applied a kappa (κ) limitation to the resampled selections to limit the influence of outliers⁷², where we retained only the resampled mean ranks within $\kappa\sigma$ of the overall average mean ($\kappa = 2$). We then recalculated the average and standard deviation of the mean rank, with the process repeated five times. All data and R code necessary to run this procedure are available at Github <https://doi.org/10.5281/zenodo.8054092>.

Disparity analyses

We evaluated coelacanth morphological disparity using two approaches. (i) We used a matrix of discrete characters (268 characters for 82 coelacanth species excluding outgroups) to explore morphological disparity based on Gower's coefficient⁷³. We plotted the morphospaces for taxa in seven time-bins: Devonian, Carboniferous, Permian, Triassic, Jurassic, Cretaceous, and extant. The first two axes of the principal coordinates analysis explained 42.01% and 11.30% of the variation, respectively (Fig. 6A). (ii) We did 2-D geometric morphometric analyses of body shape, lower jaw, and cheek region for taxa that included the relevant information. We digitized 2-D landmarks with tpsDig2 v.2.32⁷⁴ on reconstructions of coelacanths previously verified and corrected when needed. We did three separate analyses to optimize both the number of landmarks and species in each analysis. We digitized 14 2-D landmarks on 35 species to describe the lateral body outline and relative positions of the fins, 17 2-D landmarks on 34 species to capture the shape of the cheek, and seven 2-D landmarks on 38 species to describe the shape of the lower jaw (see Supplementary Information Table 2.1 for a detailed description of the landmarks). We rotated, scaled, and translated landmark coordinates with a Procrustes superimposition using the function *gpagen* in the R package *geomorph* v.4.0.1⁷⁵. We constructed morphospaces based on the two first axes of the principal component analyses. (iii) We calculated Procrustes variance for each time-bin using the function *morphol.disparity* in the package *geomorph*. All data and R code necessary to repeat disparity analyses are available at Github <https://doi.org/10.5281/zenodo.8054092>.

Reporting summary

Further information on research design is available in the Nature Portfolio Reporting Summary linked to this article.

Data availability

The CT data generated in this study have been deposited in the Morphosource database at www.morphosource.org/projects/000485769?locale=en. The phylogenetic matrix for discrete character data are available from MorphoBank (Project 3471): morphobank.org/permalink/P3471. All other data used in this study are available from the GitHub repository at <https://doi.org/10.5281/zenodo.8054092>.

Code availability

All code and data are available via <https://doi.org/10.5281/zenodo.8054092>

References

1. Zhu, M. & Yu, X. A primitive fish close to the common ancestor of tetrapods and lungfish. *Nature* **418**, 767–770 (2002).
2. Lund, R. & Lund, W. L. Coelacanths from the Bear Gulch Limestone (Namurian) of Montana and the evolution of the Coelacanthiformes. *Bull. Carnegie Mus. Nat. Hist.* **25**, 1–74 (1985).

3. Cloutier, R. Patterns, trends, and rates of evolution within the Actinistia. *Environ. Biol. Fishes* **32**, 23–58 (1991).
4. Friedman, M. & Coates, M. I. A newly recognized fossil coelacanth highlights the early morphological diversification of the clade. *Proc. R. Soc. B* **273**, 245–250 (2006).
5. Cavin, L., Piuze, A., Ferrante, C. & Guinot, G. Giant Mesozoic coelacanths (Osteichthyes, Actinistia) reveal high body size disparity decoupled from taxic diversity. *Sci. Rep.* **11**, 1–13 (2021).
6. Forey, P. L. In *The Biology of Latimeria chalumnae and Evolution of Coelacanths* (eds Musick, J. A., Bruton, M. N. & Balon, E. K.) 75–98 (1991).
7. Schaeffer, B. A study of *Diplurus longicaudatus* with notes on the body form and locomotion of the Coelacanthini. *American Museum Novitates*, **1378**, 1–32 (1948).
8. Cloutier, R. & Forey, P. L. in *Environmental Biology of Fishes* 32 59–74 (1991).
9. Forey, P. L. *History of the Coelacanth Fishes*. 419 (Chapman and Hall, 1998).
10. Toriño, P., Soto, M. & Perea, D. A comprehensive phylogenetic analysis of coelacanth fishes (Sarcopterygii, Actinistia) with comments on the composition of the Mawsoniidae and Latimeriidae: evaluating old and new methodological challenges and constraints. *Historical Biology*, <https://doi.org/10.1080/08912963.2020.1867982> (2021).
11. Schaeffer, B. A revision of *Coelacanthus newarki* and notes on the evolution of the girdles and basal plates of the median fins in the Coelacanthini. *American Museum Novitates* **1110**, 1–17 (1941).
12. Schaeffer, B. Rates of evolution in the coelacanth and dipnoan fishes. *Evolution*, 101–111 (1952).
13. Cavin, L. & Guinot, G. Coelacanths as “almost living fossils”. *Front. Ecol. Evolution* **2**, 1–5 (2014).
14. Zhu, M. et al. Earliest known coelacanth skull extends the range of anatomically modern coelacanths to the Early Devonian. *Nat. Commun.* **3**, 772 (2012).
15. Johanson, Z., Long, J. A., Talent, J. A., Janvier, P. & Warren, J. W. Oldest coelacanth, from the Early Devonian of Australia. *Biol. Lett.* **2**, 443–446 (2006).
16. Schultze, H.-P. Crossopterygians with heterocercal caudal fin from the Upper Devonian of Canada, and remains of Onychodontida from the Middle Devonian of Spain and from the Carboniferous of the USA. *Palaeontographica Abt. A* **143**, 188–208 (1973).
17. Cloutier, R. In *Devonian Fishes and Plants of Miguasha, Quebec, Canada* (eds Cloutier, R. & Schultze, H.-P.) **19**, 227–247 (Verlag Dr. Friedrich Pfeil, 1996).
18. Gess, R. W. & Coates, M. I. Fossil juvenile coelacanths from the Devonian of South Africa shed light on the order of character acquisition in actinistians. *Zool. J. Linn. Soc.* **175**, 360–383 (2015).
19. Stensiö, E. A. Über zwei Coelacanthiden aus dem Oberdevon von Wildungen. *Palaeontologischen Z.* **4**, 167–210 (1922).
20. Playford, P. E. & Lowry, D. Devonian reef complexes of the Kimberley region. *West. Aust. Geol. Surv. West. Aust.* **118**, 1–150 (1966).
21. Long, J. A. & Trinajstić, K. The Late Devonian Gogo Formation Lagerstätten of Western Australia - exceptional vertebrate preservation and diversity. *Annu. Rev. Earth Planet. Sci.* **38**, 665–680 (2010).
22. Long, J. A. & Trinajstić, K. M. A review of recent discoveries of exceptionally preserved fossil fishes from the Gogo sites (Late Devonian, Western Australia). *Earth Environ. Sci. Trans. R. Soc. Edinb.* **108**, 111–117 (2018).
23. Miles, R. S. The Holonematidae (placoderm fishes): a review based on new specimens of *Holonema* from the Upper Devonian of Western Australia. *Philos. Trans. R. Soc. Lond. (Biol.)* **263**, 101–234 (1971).
24. Moy-Thomas, J. A. & Miles, R. S. *Palaeozoic Fishes*. 2 edn, (Chapman and Hall, 1971).
25. Gardiner, B. G. & Miles, R. S. Devonian fishes of the Gogo Formation, Western Australia. *Colloq. internationaux du Cent. Natl de la Rech. Scientifique* **218**, 73–79 (1975).
26. Stensiö, E. On the Devonian coelacanthids of Germany with special reference to the dermal skeleton. *Kungliga Sven. Vetenskapsakademien Handlingar* **3** **16**, 1–67 (1937).
27. Cloutier, R. In *Early Vertebrates and Related Problems of Evolutionary Biology* (eds Chang M.-M., Liu Y.-H., & Zhang G.-R.) pp 379–428 (Science Press, 1991).
28. Northcutt, R. G. In *The mechanosensory lateral line* (eds Coombs, S., Görner, P. & Münz, H.) 17–78 (Springer, 1989).
29. Jessen, H. Weitere fischreste aus dem Oberen Plattenkalk der Bergisch-Gladbach—Paffrather mulde (Oberdevon, Rheinisches Schiefergebirge). *Palaeontogr. Abt. A Palaeozool-Stratigr.* **143**, 159–187 (1973).
30. Schaeffer, B. A coelacanth fish from the Upper Devonian of Ohio. *Sci. Publ. Clevel. Mus. Nat. Hist., N. Ser.* **1**, 1–13 (1962).
31. Millot, J. & Anthony, J. *Anatomie de Latimeria chalumnae, II - système nerveux et organes des sens*. 1–212 (CNRS, 1958).
32. Stensiö, E. The brain and the cranial nerves in fossil, lower craniate vertebrates. *Skrifter utgitt av Det Norske Videnskaps-Akademi*, 1–120 (1963).
33. Dutel, H. et al. Neurocranial development of the coelacanth and the evolution of the sarcopterygian head. *Nature* **569**, 556–559 (2019).
34. Bjerring, H. C. Yet another interpretation of the coelacanthiform basicranial muscle and its innervation. *Acta Zoologica* **74**, 289–299 (1993).
35. Mondéjar-Fernández, J., Meunier, F. J., Cloutier, R., Clément, G. & Laurin, M. A microanatomical and histological study of the scales of the Devonian sarcopterygian *Miguashaia bureaui* and the evolution of the squamation in coelacanths. *J. Anat.* **239**, 451–478 (2021).
36. Jarvik, E. in *Nobel Symposium 4: Current Problems of Lower Vertebrate Phylogeny* (ed. T. Ørving, T.) (Almqvist and Wiksells, 1968).
37. Casane, D. & Laurenti, P. Why coelacanths are not ‘living fossils’. *BioEssays* **35**, 332–338 (2013).
38. Brownstein, C. D. et al. The genomic signatures of evolutionary stasis. *Evolution* **78**, 821–834 (2024).
39. Suchard, M. et al. Bayesian phylogenetic and phylodynamic data integration using BEAST 1.10. *Virus Evolution* **4**, vey016 (2018).
40. Stadler, T. & Yang, Z. Dating phylogenies with sequentially sampled tips. *Syst. Biol.* **62**, 674–688 (2013).
41. Gavryushkina, A. et al. Bayesian total-evidence dating reveals the recent crown radiation of penguins. *Syst. Biol.* **66**, 57–73 (2017).
42. Rambaut, A., Drummond, A., Xie, D., Baele, G. & Suchard, M. Posterior summarization in Bayesian phylogenetics using Tracer 1.7. *Syst. Biol.* **67**, 901–904 (2018).
43. Drummond, A. J., Suchard, M. A., Xie, D. & Rambaut, A. Bayesian phylogenetics with BEAUti and the BEAST 1.7. *Mol. Biol. Evolution* **29**, 1969–1973 (2012).
44. Guillerme, T. dispRity: A modular R package for measuring disparity. *Methods Ecol. Evolution* **9**, 1755–1763 (2018).
45. Revell, L. phytools: An R package for phylogenetic comparative biology (and other things). *Methods Ecol. Evolution* **3**, 217–223 (2012).
46. phylotate: phylogenies with annotations v. R package version 1.3 (2019).
47. geoscale: geological time scale plotting v. R package version 2.0.1 (2022).
48. King, B. & M., R. Tip dating with fossil sites and stratigraphic sequences. *PeerJ* **8**, e9368 (2020).
49. Lewis, P. O. A likelihood approach to estimating phylogeny from discrete morphological character data. *Syst. Biol.* **50**, 913–925 (2001).

50. Yang, Z. Maximum likelihood phylogenetic estimation from DNA sequences with variable rates over sites: Approximate methods. *J. Mol. Evol.* **39**, 306–314 (1994).
51. King, B., Qiao, T., Lee, M. S. Y., Zhu, M. & Long, J. A. Bayesian morphological clock methods resurrect placoderm monophyly and reveal rapid early evolution in jawed vertebrates. *Syst. Biol.* **66**, 493–516 (2017).
52. Lemey, P., Rambaut, A., Welch, J. & Suchard, M. Phylogeography takes a relaxed random walk in continuous space and time. *Mol. Biol. Evol.* **27**, 1877–1885 (2010).
53. Drummond, A., Ho, S. Y. W., Phillips, M. J. & Rambaut, A. Relaxed phylogenetics and dating with confidence. *PLoS Biol.* **4**, e88 (2006).
54. Bielejec, F., Lemey, P., Baele, G., Rambaut, A. & Suchard, M. Inferring heterogeneous evolutionary processes through time: from sequence substitution to phylogeography. *Syst. Biol.* **63**, 493–504 (2014).
55. Goloboff, P. A. & Catalano, S. A. TNT version 1.5, including a full implementation of phylogenetic morphometrics. *Cladistics* **32**, 221–238 (2016).
56. Aberer, A. J., Krompass, D. & Stamatakis, A. Pruning rogue taxa improves phylogenetic accuracy: An efficient algorithm and Web-service. *Syst. Biol.* **62**, 162–166 (2013).
57. Marcilly, C. M., Torsvik, T. H., Domeier, M. & Royer, D. L. New paleogeographic and degassing parameters for long-term carbon cycle models. *Gondwana Res.* **97**, 176–203 (2021).
58. Marcilly, C. M., Torsvik, T. H. & Conrad, C. P. Global Phanerozoic sea levels from paleogeographic flooding maps. *Gondwana Res.* **110**, 128–142 (2022).
59. Scotese, C. R. An atlas of Phanerozoic paleogeographic maps: The seas come in and the seas go out. *Annu. Rev. Earth Planet. Sci.* **49**, 679–728 (2021).
60. Song, H., Wignall, P. B., Song, H., Dai, X. & Chu, D. Seawater temperature and dissolved oxygen over the past 500 million years. *J. Earth Sci.* **30**, 236–243 (2019).
61. Witkowski, C. R., Weijers, J. W. H., Blais, B. & Schouten, S. Molecular fossils from phytoplankton reveal secular P_{CO_2} trend over the Phanerozoic. *Sci. Adv.* **4**, eaat4556 (2018).
62. Ward, P. & Kirschvink, J. *A New History of Life: The Radical New Discoveries about the Origins and Evolution of Life on Earth.* (Bloomsbury, 2015).
63. Schachat, S. R. et al. Phanerozoic pO_2 and the early evolution of terrestrial animals. *Proc. R. Soc. B* **285**, 20172631 (2018).
64. Mills, D. B. & Canfield, D. E. Oxygen and animal evolution: Did a rise of atmospheric oxygen “trigger” the origin of animals? *BioEssays* **36**, 1145–1155 (2014).
65. McKenzie, N. R., Hughes, N. C., Gill, B. C. & Myrow, P. M. Plate tectonic influences on Neoproterozoic–early Paleozoic climate and animal evolution. *Geology* **42**, 127–130 (2014).
66. Ehleringer, J. R., Carling, T. E. & Dearing, M. D. *A History of Atmospheric CO_2 and Its Effects on Plants, Animals, and Ecosystems.* (Springer, 2005).
67. Newell, R. C. Effect of temperature on the metabolism of poikilotherms. *Nature* **212**, 426–428 (1966).
68. Wright, D. F. & Stigall, A. L. Geologic drivers of Late Ordovician faunal change in Laurentia: Investigating links between tectonics, speciation, and biotic invasions. *PLoS ONE* **8**, e68353 (2013).
69. Miguel, R., Gallo, V. & Morrone, J. J. Distributional patterns of †Mawsoniidae (Sarcopterygii: Actinistia). *An. da Acad. brasileira de Ciências* **86**, 159–170 (2014).
70. Cupello, C. et al. The long-time adaptation of coelacanths to moderate deep water: reviewing the evidences. *Bull. Kitakyushu Mus. Nat. Hist. Hum. Hist.* **17**, 29–35 (2019).
71. Hijmans, R. J., Phillips, S., Leathwick, J. & Elith, J. dismo: Species Distribution Modeling. R package version 1.1-4. *CRAN.R-project.org/package=dismo.* (2017).
72. Bradshaw, C. J. A. & Brook, B. W. How to rank journals. *PLoS One* **11**, e0149852 (2016).
73. Gower, J. C. A general coefficient of similarity and some of its properties. *Biometrics* **27**, 857–871 (1971).
74. tpsDig program v. version 2.32 (Ecology and evolution, SUNY at Stony Brook, 2018).
75. *Geometric morphometric analyses of 2D and 3D landmark data (geomorph)* (2021).

Acknowledgements

We acknowledge the Goonyandi people and other landholders on which the Gogo fish sites are located. Members of the 2008 field team are thanked for their contribution. Tim Senden, Mike Turner (Australian National University, Australia), and Ruth Williams (Adelaide Microscopy, Australia) are thanked for performing the CT scans. Michael Siverson and Helen Ryan (Western Australian Museum) are thanked for arranging specimen access. Jenjira Prombansung, Clara Comeau, Chantal Rodrigue, and Laurent Houle (UQAR, Canada) helped with illustrations. Richard Flament and Laurianne Richard assisted with compiling coelacanth diversity data. Wen Wen provided high resolution images of specimens for scoring characters. Andrew Wendruff and Mark V.H. Wilson for the permission to use information on unpublished *Whiteia* coelacanths. Florian Witzmann (Museum für Naturkunde, Germany) is thanked for access to *Euporosteus eifeliensis* and cast material of *Diplocercides kayseri*. Fieldwork was funded by the Australian Research Council, with grant DP 0772138 (JAL). This work was supported by the Australian Research Council DP 220100825 (JAL, KT, AMC), DP 200103398 (JAL, AMC), DP 110101127 (JAL, KT) and DP 0772138 (JAL). Other fundings sources include Honorary Visiting Scholar at Flinders University 2019, 2023 to (RC), Visiting professor at Mahasarakham University (2023 to RC), and Natural Sciences and Engineering Research Council of Canada RGPIN–2019–06133 (RC), NERC (Natural Environment Research Council) Standard Grant NE/P013090/1 (HD), and QEII Fellowship (KT).

Author contributions

Conceived project: A.M.C., R.C., K.T., J.A.L. Fieldwork: A.M.C., K.T., J.A.L. Specimen preparation & photography: A.M.C., K.T., J.A.L. Specimen interpretation: A.M.C., R.C., H.D., J.A.L. CT –scanning, segmentation & visualisation: A.M.C. Matrix construction: A.M.C., R.C., J.A.L. Character scoring: A.M.C., R.C., H.D., B.K., J.A.L., O.V. Analyses: R.C., M.S.Y.L., B.K., O.V., C.J.A.B. Figures: A.M.C., R.C., M.S.Y.L., B.K., J.A.L., O.V., C.J.A.B. Writing – original draft: A.M.C., R.C., J.A.L. Writing – review & editing: A.M.C., R.C., M.S.Y.L., H.D., B.K., K.T., J.A.L., O.V., C.J.A.B.

Competing interests

The authors declare no competing interests.

Additional information

Supplementary information The online version contains supplementary material available at <https://doi.org/10.1038/s41467-024-51238-4>.

Correspondence and requests for materials should be addressed to Alice M. Clement.

Peer review information *Nature Communications* thanks Lauren Sallan, Piotr Szrek and Min Zhu for their contribution to the peer review of this work. A peer review file is available.

Reprints and permissions information is available at <http://www.nature.com/reprints>

Publisher’s note Springer Nature remains neutral with regard to jurisdictional claims in published maps and institutional affiliations.

Open Access This article is licensed under a Creative Commons Attribution-NonCommercial-NoDerivatives 4.0 International License, which permits any non-commercial use, sharing, distribution and reproduction in any medium or format, as long as you give appropriate credit to the original author(s) and the source, provide a link to the Creative Commons licence, and indicate if you modified the licensed material. You do not have permission under this licence to share adapted material derived from this article or parts of it. The images or other third party material in this article are included in the article's Creative Commons licence, unless indicated otherwise in a credit line to the material. If material is not included in the article's Creative Commons licence and your intended use is not permitted by statutory regulation or exceeds the permitted use, you will need to obtain permission directly from the copyright holder. To view a copy of this licence, visit <http://creativecommons.org/licenses/by-nc-nd/4.0/>.

© The Author(s) 2024